Environmental Science & Technology Letters

pubs.acs.org/journal/estlcu

Letter

Satellites Detect a Methane Ultra-emission Event from an Offshore Platform in the Gulf of Mexico

Itziar Irakulis-Loitxate,*[,‖] Javier Gorroño,[‖] Daniel Zavala-Araiza, and Luis Guanter

Cite This: *Environ. Sci. Technol. Lett.* 2022, 9, 520−525

Read Online

ACCESS | Metrics & More | Article Recommendations | Supporting Information

ABSTRACT: Mitigation of methane emissions from fossil fuel extraction, processing, and transport is one of the most effective ways to slow global warming. Satellite-based methods are instrumental for the detection, characterization, and quantification of this type of emissions. However, despite the rapid development of satellite-based methane plume detection methods for terrestrial surfaces, there is still an important observational gap with respect to offshore oil and gas infrastructure, which accounts for roughly 30% of global production. In this work, we have used observations from the WorldView-3 and Landsat 8 satellite missions in a particular observation-illumination geometry to image offshore methane plumes from space. The study site is an offshore oil and gas production platform in the Gulf of Mexico, near the coast of Campeche, in one of Mexico's major oil producing fields. Our data suggest that the platform vented high volumes of methane during a 17-day ultra-emission event, amounting to 0.04 ± 0.01 Tg of methane (equivalent to 3.36 million tons of carbon dioxide) released to the atmosphere if integrated over time. Our results illustrate how satellites can detect methane plumes from offshore infrastructure, which represents a significant breakthrough in the monitoring of industrial methane emissions from space.

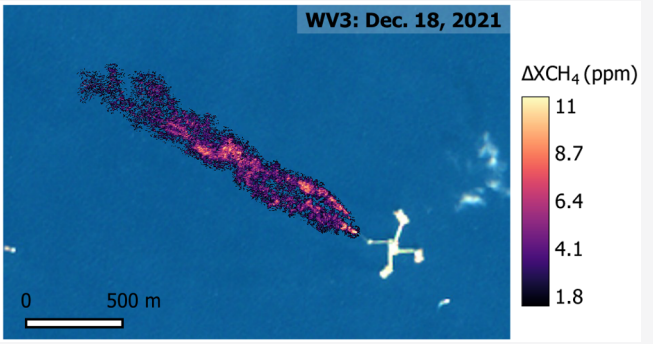

KEYWORDS: *Methane emissions, offshore platforms, high-resolution satellite data, WorldView-3, Landsat 8, Gulf of Mexico, sun-glint, VIIRS*

INTRODUCTION

Methane (CH_4) is the second most important anthropogenic greenhouse gas.[1] Significantly reducing CH_4 emissions has been recognized as an essential opportunity in order to reduce the rate of global warming in the short and medium terms.[2,3] However, emitting sectors have significant uncertainty about the amount, location, and duration of emissions.[4] Among them, the emissions derived from the oil and gas (O&G) sector stand out,[5,6] since a large fraction of these emissions can be reduced with currently available, highly cost-effective technologies.[7]

In order to mitigate these emissions as soon as possible, great efforts are being made to develop more efficient monitoring methods for O&G infrastructure. New methods in CH_4 emission detection from high- and mid-resolution satellites have successfully demonstrated their effectiveness in numerous studies.[8−14] For example, GHGSat, Sentinel-2 (S2), Landsat, PRISMA, Gaofen5, ZY1-AHSI, and WorldView3 (WV3) satellites measuring backscattered solar radiation in the short-wave infrared (SWIR) spectral region have demonstrated a detection capability of at least ∼30−1800 kg CH_4/h for a range of continental O&G extraction regions.[9,12,14,15] However, at the time of this study, none of those satellite systems has been shown to be capable of detecting emissions from offshore O&G operations. This represents a strong limitation in our capability to monitor industrial CH_4 emissions from space, as offshore O&G production constitutes about 28% of the world's total O&G production.[16,17]

The satellites limitations to detect CH_4 over water has led to a lower number of measurement-based, top-down studies, mostly performed from airplanes or ships, resulting in temporally constrained emission characterization and making it challenging to monitor intermittent emission events.[18−22]

The main difficulty for the detection of offshore CH_4 emissions from space is the high absorption of SWIR radiation by water, which limits the amount of reflected light reaching the sensor and, subsequently, the capability of these sensors to disentangle the absorption of CH_4 in the SWIR from instrument noise and sea surface roughness. However, this limitation can be overcome by satellites measuring solar radiation specularly reflected by the water surface in the so-

Received: April 4, 2022
Revised: May 24, 2022
Accepted: May 25, 2022
Published: June 1, 2022

https://doi.org/10.1021/acs.estlett.2c00225
Environ. Sci. Technol. Lett. 2022, 9, 520−525

called sun-glint observation mode[23] (Materials and Methods). For this type of observation, the sensor must point to the forward scattering direction of the Sun-target plane. This can be achieved by pointing the platform accordingly in the case of agile platforms (e.g., the case of WorldView-3, GHGSat, and PRISMA missions) or by using the part of the image located opposite to the Sun in the case of sensors without pointing ability but with relatively large fields of view (e.g., Sentinel-2 and Landsat 8).

In this work, we have explored the ability of satellite-based optical imagers for the detection of CH_4 plumes emitted from offshore O&G infrastructure using sun-glint mode acquisitions. We have used data acquired by the WorldView-3 (WV3) SWIR and Landsat 8 (L8) missions to detect and quantify strong CH_4 plumes from an offshore platform in the Gulf of Mexico. These CH_4 plume detections have been combined with satellite-based data of flaring activity from the same platform for analyses of the emission source and duration.

MATERIALS AND METHODS

Study Area. The initial objective of the study was to explore the feasibility of offshore CH_4 plume detection with the WV3 satellite system. An area with potentially frequent and strong emissions was needed for this experiment. On the basis of the recent analysis of offshore emissions by Zavala-Araiza et al.,[19] we selected a study site on the Mexican side of the Gulf of Mexico, near the coast of Campeche. This is the Zaap offshore field area, which is responsible for roughly 20% of Mexican oil offshore production.[24]

The site with detected emissions is the Zaap-C platform, whose main processes include O&G production through a series of wells and first stage separation, in addition to a power generation unit used for gas injection. There are two boom-type flares linked to the production and separation units, which were the sources of emissions detected in this work.

Satellite Data Sets. WV3 is a multispectral satellite with eight bands in the SWIR region and 3.7 m spatial resolution. It also includes eight bands in the VNIR region, but we do not have those data for this study, as they are provided as a separate product. The very high spatial resolution combined with the high SNR makes it possible to pinpoint the emission source with high precision.[14] The satellite incorporates an agile system that can deliver better than a daily revisit over critical infrastructure and is relatively free to adapt the angular configuration close to the sun-glint. On the other hand, its data are on demand, so it is only helpful for monitoring potential emitters with a known location. The first WV3 SWIR data set from our study site that we could use for CH_4 mapping (cloud free and proper angular configuration) was acquired in December 2021.

The detection of a strong emission from one of the platforms inside the imaged area motivated a further analysis of the emissions of that platform using open-access multispectral satellites with global coverage, which have also been shown to have sensitivity to CH_4.[12] Because of the particular characteristics of the orbit, we could track emissions from the platform using archive data from the L8 between 2013 and January 2022. This was not possible for the S2 platform, as our study site did not fall inside the forward scattering region of the S2 swath (Figure S2).

Emission Detection and Quantification. We have detected the offshore CH_4 emissions using the WV3 and L8 high-resolution satellites. The first step is the derivation of CH_4 concentration enhancement (ΔXCH_4) maps.

In our case, the Gulf of Mexico images have a near-optimum angular configuration for the L8 Operational Land Imager (OLI) instrument (Section S1, Figure S1), which implies a detection limit sufficient for these extreme emissions.[25]

The relative spectral homogeneity of the ocean scene simplified the ΔXCH_4 retrieval algorithm. In both cases, the applied ΔXCH_4 retrieval method is based on the simple band ratio between a band sensitive to CH_4 and a spectrally close band with no sensitivity (or minimum sensitivity). In WV3, we have used band B8 as the band with the highest sensitivity and B5 as the closest band with the lowest sensitivity and in L8 OLI bands B7 and B6 in the same order. The bands B5 of WV3 and B6 of L8 contain residual sensitivities to CH_4 transmittance that is compensated during retrieval (see Section S2 for more information).

Once we obtained the ΔXCH_4 enhancement map, we have performed a plume masking to select CH_4 plume pixels and quantify the emission (Figure S4). Finally, we have converted the selected pixels into flux rates (Q) applying the IME method.[8] To do so, we have used 1 h average 10 m wind (U10) data from the NASA GEOS-FP meteorological reanalysis product at $0.25° \times 0.3125°$ resolution[26] (see Section S2 for more information about the CH_4 detection and quantification methodology).

Verification of CH_4 Plume Detections. Taking advantage of the almost simultaneous overpass of S2 and WV3 on the same day with 3 min and 51 s difference, we have compared both data products to verify different properties of the emission environment. The S2 data provide additional information layers (e.g., RGB and water vapor) that support the identification of possible error sources (surface artifacts, water roughness changes, water vapor, or smoke). For example, the B9/B8A band ratio of S2 enhances water vapor but not CH_4. Thus, we can verify that the water vapor columns emitted from some flares are not related to the detected CH_4 plumes (Section S4, Figure S9).

In the case of L8, this verification can be performed from the RGB composition of the same image (Section S4, Figure S10).

Moreover, we have tested WV3 CH_4 retrieval against simulated products based on CH_4 plumes generated from WRF-LES simulations (Section S3). These simulations have helped us estimate a WV3 detection limit for that image, i.e., the minimum detectable emission flux at that location under those conditions and with the angular configuration of this particular image, which is close to the sun-glint but not optimal (Figure S1).

Flaring Activity Tracking. We have monitored the emission source flaring activity mainly using the Fire Information for Resource Management System (FIRMS) web[27] platform's VIIRS data (Suomi NPP and NOAA-20). Using the viewer, we have checked the data from the official VIIRS Fires and Thermal Anomalies product of both satellites on the platform's location and extracted the fire radiative power (FRP) value. At the same time, we checked if the days without data were due to clouds or not looking at the RGB data of each of the two satellites. These data provide daily diurnal and nocturnal information at a 375 m spatial resolution. This resolution provides errors of several meters in the attribution of flaring source coordinates; however, the offshore platforms are sufficiently scattered in the scene to

https://doi.org/10.1021/acs.estlett.2c00225
Environ. Sci. Technol. Lett. 2022, 9, 520−525

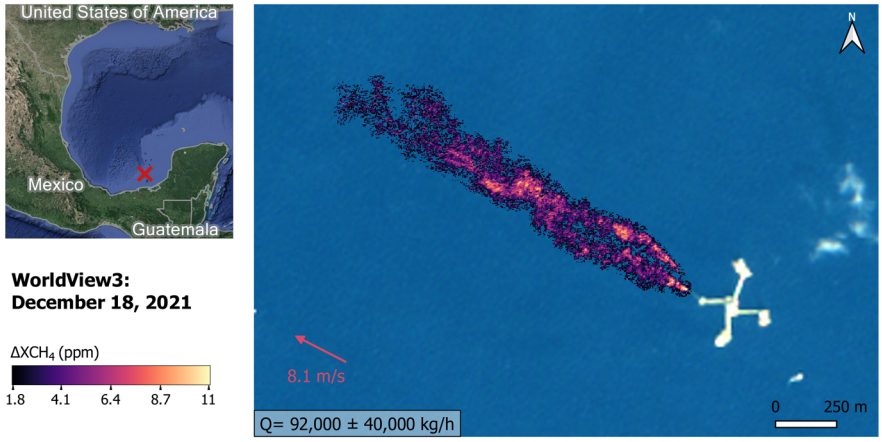

Figure 1. Main panel shows a CH_4 plume from an offshore platform as detected with the WV3 satellite on December 18, 2021. The background image is from a S2 data acquisition from a contiguous noncloudy day. The map on the left panel indicates the location of the platform in the Gulf of Mexico: latitude 19.5658°, longitude −92.2367° (source map from Google Earth).

attribute the flaring signal with large confidence to each one of them.

RESULTS AND DISCUSSION

Using WV3 and L8 multispectral satellite SWIR data, we have detected CH_4 plumes at three different dates from the Zaap-C offshore platform (Figure 1 and Figure S10).

Figure 2 shows the temporal evolution of the flaring at this installation. There, we can appreciate near-constant flare activity over several weeks preceding the event, until the flare is suddenly turned off from December 8 until December 27. Nonetheless, the flare was also lit up sporadically during this switch-off period: in the daytime on the 16th and 17th of December and at night on the 17th, 24th, and 26th, which indicates short-duration, intermittent flaring activity. There is no daily information from S2 and L8, but the analysis of their fire-sensitive bands (high emissivity of fire bands B12 and B7, respectively) confirms a flaring stop from day 8 (first day without flaring) to day 28 (first day with flaring after the event).

Therefore, from December 8 to December 27, we have a total of 17 days (excluding days 16 and 17 and the nights of 17, 24, and 26) on which the facility kept the flaring off. The three detected plumes are especially well located within this period, covering the event's beginning, middle, and near end (Figure 2). Considering that the three plumes have a very similar emission flux (111,000 ± 45,000 kg/h, 92,000 ± 40,000 kg/h, 94,000 ± 38,000 kg/h), we obtain an average emission flux of 99,000 ± 24,000 kg/h assuming no correlation between the estimates. If we consider that the platform was emitting during the whole event with a relatively constant flux, as the three detections suggest, we obtain an integrated total emission of 0.04 ± 0.01 Tg of CH_4 in the whole event, equivalent to 3.36 million tons of carbon dioxide (using 84 as the 20 year global warming potential factor). This has been calculated as follows:

$$15\,\text{days} \times 24\,\text{h} + 4\,\text{days} \times 12\,\text{h} = 408\,\text{h}$$

$$\rightarrow 408\,\text{h} \times 99{,}000\,\text{kg/h} = 40{,}000{,}000 \pm 10{,}000{,}000\,\text{kg}$$

In this estimation, we consider that on the dates without flaring during the day and night, the source was emitting for 24 h, and on the days with flaring during the night but not the day, or vice versa, it emitted for 12 h.

An event of this magnitude is equivalent to roughly 3% of Mexico's O&G emissions (1.3 Tg/yr), although the total magnitude of Mexico's emissions would also be higher if such events happened frequently enough. This single event would have a similar magnitude to the entire measurement-based estimate of regional emissions from Mexico's offshore region (0.044 Tg/yr), according to the Shen et al. 2021[28] and Zavala-Araiza et al. 2021[19] studies.

Although we only show a time series from November 1 to January 27 in Figure 2, the entire VIIRS series (since January 2012) shows very consistent flaring activity at this facility over the years, with few noncloudy days without flaring data, and the Landsat satellite time series show active flaring since 2008 without a single clear sky day without flaring. Therefore, we deduce that this ultra-emitting event—likely related to abnormal process conditions (e.g., malfunctions or equipment issues) at the site that result in substantial vented gas through the flare —is a one-time incident and with the longest duration since flaring activity began at this platform. Linking the detection and characterization approach in this study with process and site-level operating conditions could shed light into the causes behind high-emitting events. Such monitoring on a larger data set of offshore high-emitting events would provide knowledge of root causes and emission reduction opportunities.

The magnitude of the quantified emission rates through this event differ from those reported in other offshore studies and campaigns,[18,19,29] where the highest emissions do not exceed ∼3800 kg/h.[18] This may be due to the intermittent nature of flare malfunctions, the relatively small sample size of currently available measurement-based studies, or because the detection methods (airplane, ship, or drone) used in these campaigns sometimes require a prewarning to the platform operators so that they could anticipate and operate with greater attention the state of the installations. These stochastic events are likely to be unaccounted for current inventories, and if they occur frequently enough, they represent a significant contribution to total emissions for the offshore sector. In the case of Mexican offshore emissions, recent studies[19,28] pointed at a significant overestimation of the national inventory when compared to measurement-based estimates. Nonetheless, these measurement campaigns may underestimate the real magnitude of the offshore emissions by not including ultra-emissions such as the

https://doi.org/10.1021/acs.estlett.2c00225
Environ. Sci. Technol. Lett. 2022, 9, 520−525

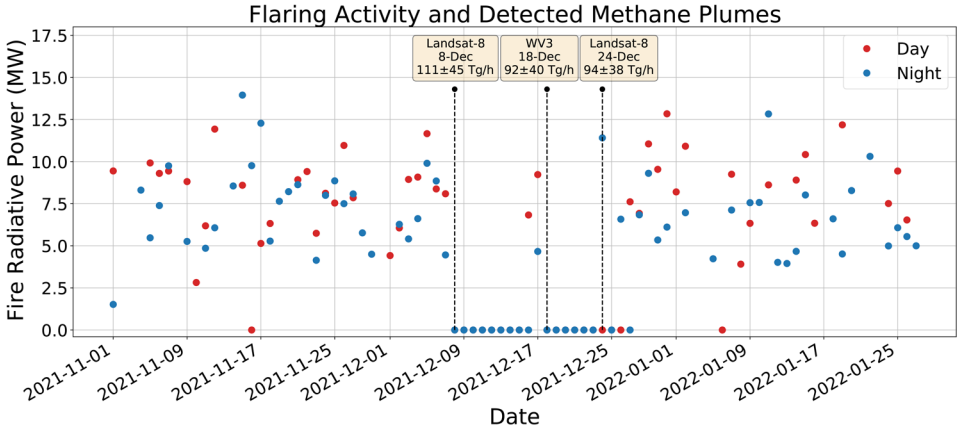

Figure 2. Time series of flaring activity at the offshore platform responsible for the detected methane plumes. Flaring has been plotted as the average value of fire radiative power (in megawatts) detected by VIIRS/NOAA-20 and VIIRS/Suomi-NPP. The red dots represent the average value of fire radiative power during the day and the blue dots the night value. The missing data are due to cloudy dates. The vertical lines indicate the day when the emissions were detected.

one presented here. In that case, the difference between the estimates from the studies and the official inventories could be compensated.

Our work demonstrates the importance of having robust methods that transparently monitor these events. Further work is needed to better understand the prevalence of such events and what fraction of emissions, relative to the total, they represent.

In absence of stringent, measurement-based reporting frameworks, events like this one could easily go unnoticed. The high-resolution acquisitions from these two satellites have proven to be sufficient to attribute the emission to a specific source accurately, even if the plume is located over water. In the case of WV3, its 3.7 m/pix resolution makes it possible to distinguish two plumes emanating from the same installation, which then converge into a single plume downwind. These two sources are probably associated to the two flares at different sections of the platform (i.e., drilling and separation). In the case of L8 OLI, the 30 m resolution is sufficient to detect the origin of the emission and a defined plume. Although the L8 overpass at this offshore platform provides optimum viewing angular conditions (Figures S1 and S10), the occurrence of the emission during the winter means that the sun zenith angle is substantially high. A better angular configuration would occur closer to the summer solstice, which is expected to reduce the detection limit substantially.

Finally, from the WV3 image simulations, we have estimated that the detection limit of this satellite is around 1500 kg/h for this scene (Section S3). However, the detection limit over oceans mainly depends on the angular configuration of the acquisition. Even though this acquisition is close to the sun-glint angular configuration, there is certainly room for improvement. That is, it is possible to establish a tradeoff between the target revisit and detection limit in order to define a specific acquisition strategy. Moreover, it is also expected that the detection limit can be further reduced over this same region for other periods of the year with more favorable solar geometries. Since the O&G emitters usually follow a long tail distribution (a few sources emit most of the emissions), both onshore and offshore, a lower detection limit would allow identifying most of the emitters detected in previous occasions in the Mexican Gulf of Mexico[19] or disproportionately high emission events that are quite frequent in the United States Gulf of Mexico.[18] On the other hand, it should be noted that other factors could strongly affect the detection capability of satellites. The most prominent are the wind speed (the higher the wind speed is, the higher the detection limit is), which is mostly high at sea, and the roughness of the sea due to waves (the higher the roughness/waves, the more difficult it will be to detect emissions).[29,30] Due to these last two characteristics, it is expected that the methods used here to detect offshore emissions in the ocean will obtain even better results in lakes (ideal case) and seas with very calm waters, where waves and wind are much lower.

Our results show that offshore CH_4 monitoring efforts can be improved if they are combined with flaring activity data, as a break in flaring activity can indicate a possible malfunction event. Similarly, it would be useful to combine the observations used in this study with data from other satellites with lower spatial resolution, such as ESA's TROPOMI sensor, which, since November 2021, provides data on the sun-glint areas of the oceans.[31] Unfortunately, the Gulf of Mexico is outside the sun-glint area during the study period, so we could not get complementary information from TROPOMI. Landsat and S2 satellite continuous data collection combined with an updated database of offshore facility locations could provide continuous monitoring of ultra-emissions. However, monitorable areas would be limited to the orbit fringe that meets near-sun-glint characteristics. A database of potential facilities would pave the way for automated emission detection, reducing the possibility of mistaking an ultra-emission for a false positive. However, current retrieval methods do not allow for fully automatic monitoring without supervision that the potential plume detection and masking have been done correctly, and therefore, the quantification is correct (Section 2, Figure S4).

The plumes presented in this work demonstrate that the detection of CH_4 emissions in the ocean is already possible from space and that we can even monitor them over time as long as scenes are acquired with an adequate angular configuration. The list of satellites with ability for offshore CH_4 mapping can be extended by the PRISMA hyperspectral system and the upcoming EnMAP, MethaneSAT, and Carbon Mapper missions, whose spectral configurations and pointing abilities meet the requirements for detecting CH_4 over water.

https://doi.org/10.1021/acs.estlett.2c00225
Environ. Sci. Technol. Lett. 2022, 9, 520−525

These findings represent a new breakthrough in the quickly developing field of high-resolution CH_4 mapping from space.

■ ASSOCIATED CONTENT

Supporting Information

Additional background data, information on the image angular configuration, detailed information on the implemented methane retrieval and validation methodology, complementary images and data on the emission verification, and images of the Landsat 8 detected emissions. This work has been previously submitted to a preprint version repository: Irakulis-Loitxate, I; Gorroño, J; Zavala-Araiza, D; Guanter, L; Satellites detect a methane ultra-emission event from an offshore platform in the Gulf of Mexico. 2022. EarthArXiv. 10.31223/X5504G (accessed May 22, 2022). The Supporting Information is available free of charge at https://pubs.acs.org/doi/10.1021/acs.estlett.2c00225.

(PDF)

■ AUTHOR INFORMATION

Corresponding Author

Itziar Irakulis-Loitxate − *Research Institute of Water and Environmental Engineering (IIAMA), Universitat Politècnica de València (UPV), 46022 Valencia, Spain;* orcid.org/0000-0003-3646-4950; Email: iiraloi@doctor.upv.es

Authors

Javier Gorroño − *Research Institute of Water and Environmental Engineering (IIAMA), Universitat Politècnica de València (UPV), 46022 Valencia, Spain*

Daniel Zavala-Araiza − *Environmental Defense Fund, 1017 LN Amsterdam, The Netherlands; Institute for Marine and Atmospheric Research Utrecht, Utrecht University, 3584 CC Utrecht, The Netherlands;* orcid.org/0000-0002-8394-5725

Luis Guanter − *Research Institute of Water and Environmental Engineering (IIAMA), Universitat Politècnica de València (UPV), 46022 Valencia, Spain; Environmental Defense Fund, 1017 LN Amsterdam, The Netherlands;* orcid.org/0000-0002-8389-5764

Complete contact information is available at: https://pubs.acs.org/10.1021/acs.estlett.2c00225

Author Contributions

‖I. Irakulis-Loitxate and J. Gorroño contributed equally.

Author Contributions

The manuscript was written through contributions of all authors. All authors have given approval to the final version of the manuscript.

Notes

The authors declare no competing financial interest.

■ ACKNOWLEDGMENTS

The authors thank the European Space Agency and European Space Imaging for access to WV3 data through the third-party mission plan. Javier Gorroño is funded by an ESA Living Planet Fellowship (ESA Contract No. 4000130980/20/I-NS). Authors Itziar Irakulis-Loitxate, Javier Gorroño, and Luis Guanter received funding from ESA contract 4000134929. Elena Sánchez-García is thanked for her support for the selection of the study site, and Maxar Technologies, Inc., for the acquisition of WV3 SWIR data for this study.

■ REFERENCES

(1) Etminan, M.; Myhre, G.; Highwood, E. J.; Shine, K. P. Radiative Forcing of Carbon Dioxide, Methane, and Nitrous Oxide: A Significant Revision of the Methane Radiative Forcing. *Geophys. Res. Lett.* **2016**, DOI: 10.1002/2016GL071930.

(2) Nature Editors. Control Methane to Slow Global Warming — Fast. *Nature* **2021**, *596* (7873), 461.

(3) *Global Methane Assessment: Benefits and Costs of Mitigating Methane Emissions*; United Nations Environment Programme and Climate and Clean Air Coalition: Nairobi, 2021.

(4) Saunois, M.; Stavert, A. R.; Poulter, B.; Bousquet, P.; Canadell, J. G.; Jackson, R. B.; Raymond, P. A.; Dlugokencky, E. J.; Houweling, S.; Patra, P. K.; Ciais, P.; Arora, V. K.; Bastviken, D.; Bergamaschi, P.; Blake, D. R.; Brailsford, G.; Bruhwiler, L.; Carlson, K. M.; Carrol, M.; Castaldi, S.; Chandra, N.; Crevoisier, C.; Crill, P. M.; Covey, K.; Curry, C. L.; Etiope, G.; Frankenberg, C.; Gedney, N.; Hegglin, M. I.; Hoglund-Isaksson, L.; Hugelius, G.; Ishizawa, M.; Ito, A.; Janssens-Maenhout, G.; Jensen, K. M.; Joos, F.; Kleinen, T.; Krummel, P. B.; Langenfelds, R. L.; Laruelle, G. G.; Liu, L.; Machida, T.; Maksyutov, S.; McDonald, K. C.; McNorton, J.; Miller, P. A.; Melton, J. R.; Morino, I.; Muller, J.; Murguia-Flores, F.; Naik, V.; Niwa, Y.; Noce, S.; O'Doherty, S.; Parker, R. J.; Peng, C.; Peng, S.; Peters, G. P.; Prigent, C.; Prinn, R.; Ramonet, M.; Regnier, P.; Riley, W. J.; Rosentreter, J. A.; Segers, A.; Simpson, I. J.; Shi, H.; Smith, S. J.; Steele, L. P.; Thornton, B. F.; Tian, H.; Tohjima, Y.; Tubiello, F. N.; Tsuruta, A.; Viovy, N.; Voulgarakis, A.; Weber, T. S.; van Weele, M.; van der Werf, G. R.; Weiss, R. F.; Worthy, D.; Wunch, D.; Yin, Y.; Yoshida, Y.; Zhang, W.; Zhang, Z.; Zhao, Y.; Zheng, B.; Zhu, Q.; Zhu, Q.; Zhuang, Q. The Global Methane Budget 2000−2017. *Earth Syst. Sci. Data* **2020**, *12*, 1561.

(5) *Oil and Gas Methane Partnership (OGMP) 2.0 Framework*; United Nations Environment Programme and Climate and Clean Air Coalition, 2020; pp 1−18.

(6) Lauvaux, T.; Giron, C.; Mazzolini, M.; d'Aspremont, A.; Duren, R.; Cusworth, D.; Shindell, D.; Ciais, P. Global Assessment of Oil and Gas Methane Ultra-Emitters. *Science* **2022**, *375*, 557−561.

(7) Ocko, I. B.; Sun, T.; Shindell, D.; Oppenheimer, M.; Hristov, A. N.; Pacala, S. W.; Mauzerall, D. L.; Xu, Y.; Hamburg, S. P. Acting Rapidly to Deploy Readily Available Methane Mitigation Measures by Sector Can Immediately Slow Global Warming. *Environ. Res. Lett.* **2021**, *16* (5), 054042.

(8) Varon, D. J.; Jacob, D. J.; Mckeever, J.; Jervis, D.; Durak, B. O. A.; Xia, Y.; Huang, Y. Quantifying Methane Point Sources from Fine-Scale Satellite Observations of Atmospheric Methane Plumes. *Atmos. Meas. Tech* **2018**, *11*, 5673−5686.

(9) Irakulis-Loitxate, I.; Guanter, L.; Liu, Y.-N.; Varon, D. J.; Maasakkers, J. D.; Zhang, Y.; Chulakadabba, A.; Wofsy, S. C.; Thorpe, A. K.; Duren, R. M.; Frankenberg, C.; Lyon, D. R.; Hmiel, B.; Cusworth, D. H.; Zhang, Y.; Segl, K.; Gorroño, J.; Sánchez-García, E.; Sulprizio, M. P.; Cao, K.; Zhu, H.; Liang, J.; Li, X.; Aben, I.; Jacob, D. J. Satellite-Based Survey of Extreme Methane Emissions in the Permian Basin. *Sci. Adv.* **2021**, *7* (27), eabf4507.

(10) Varon, D. J.; Jervis, D.; McKeever, J.; Spence, I.; Gains, D.; Jacob, D. J. High-Frequency Monitoring of Anomalous Methane Point Sources with Multispectral Sentinel-2 Satellite Observations. *Atmos. Meas. Tech.* **2021**, *14* (4), 2771−2785.

(11) Guanter, L.; Irakulis-Loitxate, I.; Gorroño, J.; Sánchez-garcía, E.; Cusworth, D. H.; Varon, D. J.; Cogliati, S.; Colombo, R. Mapping Methane Point Emissions with the PRISMA Spaceborne Imaging Spectrometer (Under Review). *Remote Sens. Environ.* **2021**, *265*, 112671.

(12) Irakulis-Loitxate, I.; Guanter, L.; Maasakkers, J. D.; Zavala-Araiza, D.; Aben, I. Satellites Detect Abatable Super-Emissions in One of the World's Largest Methane Hotspot Regions. *Environ. Sci. Technol.* **2022**, *56*, 2143−2152.

(13) Cusworth, D. H.; Duren, R. M.; Thorpe, A. K.; Pandey, S.; Maasakkers, J. D.; Aben, I.; Jervis, D.; Varon, D. J.; Jacob, D. J.; Randles, C. A.; Gautam, R.; Omara, M.; Schade, G. W.; Dennison, P. E.; Frankenberg, C.; Gordon, D.; Lopinto, E.; Miller, C. E.

Multisatellite Imaging of a Gas Well Blowout Enables Quantification of Total Methane Emissions. *Geophys. Res. Lett.* **2021**, DOI: 10.1029/2020GL090864.
(14) Sánchez-García, E.; Gorroño, J.; Irakulis-Loitxate, I.; Varon, D.; Guanter, L. Mapping Methane Plumes at Very High Spatial Resolution with the WorldView-3 Satellite. *Atmos. Meas. Tech.* **2022**, *15*, 1657−1674.
(15) Varon, D.; Jervis, D.; McKeever, J.; Spence, I.; Gains, D.; Jacob, D. High-Frequency Monitoring of Anomalous Methane Point Sources with Multispectral Sentinel-2 Satellite Observations. *Atmos. Meas. Tech. Discuss.* **2021**, *14*, 2771−2785.
(16) Distribution of onshore and offshore crude oil production worldwide from 2005 to 2025. *Statista*. https://www.statista.com/statistics/624138/distribution-of-crude-oil-production-worldwide-onshore-and-offshore/ (accessed Jan 27, 2022).
(17) Your Energy Knowledge House. *Rystad Energy*. https://www.rystadenergy.com/ (accessed Apr 18, 2021).
(18) Gorchov Negron, A. M.; Kort, E. A.; Conley, S. A.; Smith, M. L. Airborne Assessment of Methane Emissions from Offshore Platforms in the U.S. Gulf of Mexico. *Environ. Sci. Technol.* **2020**, *54* (8), 5112−5120.
(19) Zavala-Araiza, D.; Omara, M.; Gautam, R.; Smith, M. L.; Pandey, S.; Aben, I.; Almanza-Veloz, V.; Conley, S.; Houweling, S.; Kort, E. A.; Maasakkers, J. D.; Molina, L. T.; Pusuluri, A.; Scarpelli, T.; Schwietzke, S.; Shen, L.; Zavala, M.; Hamburg, S. P. A Tale of Two Regions: Methane Emissions from Oil and Gas Production in Offshore/Onshore Mexico A Tale of Two Regions: Methane Emissions from Oil and Gas Production in Offshore/Onshore Mexico. *Environ. Res. Lett* **2021**, *16*, 024019.
(20) Yacovitch, T. I.; Daube, C.; Herndon, S. C. Methane Emissions from Offshore Oil and Gas Platforms in the Gulf of Mexico. *Environ. Sci. Technol.* **2020**, *54* (6), 3530−3538.
(21) Foulds, A.; Allen, G.; Shaw, J. T.; Bateson, P.; Barker, P. A.; Huang, L.; Pitt, J. R.; Lee, J. D.; Wilde, S. E.; Dominutti, P.; Purvis, R. M.; Lowry, D.; France, J. L.; Fisher, R. E.; Fiehn, A.; Puhl, M.; Bauguitte, S. J. B.; Conley, S. A.; Smith, M. L.; Lachlan-Cope, T.; Pisso, I.; Schwietzke, S. Quantification and Assessment of Methane Emissions from Offshore Oil and Gas Facilities on the Norwegian Continental Shelf. *Atmos. Chem. Phys.* **2022**, *22*, 4303−4322.
(22) France, J. L.; Bateson, P.; Dominutti, P.; Allen, G.; Andrews, S.; Bauguitte, S.; Coleman, M.; Lachlan-Cope, T.; Fisher, R. E.; Huang, L.; Jones, A. E.; Lee, J.; Lowry, D.; Pitt, J.; Purvis, R.; Pyle, J.; Shaw, J.; Warwick, N.; Weiss, A.; Wilde, S.; Witherstone, J.; Young, S. Facility Level Measurement of Offshore Oil and Gas Installations from a Medium-Sized Airborne Platform: Method Development for Quantification and Source Identification of Methane Emissions. *Atmos. Meas. Tech.* **2021**, *14* (1), 71−88.
(23) Larsen, N. F.; Stamnes, K. H. Methane Detection from Space: Use of Sunglint. *Opt. Eng.* **2006**, *45* (1), 016202.
(24) Sistema de Información de Hidrocarburos (SIH). *CNIH*. https://sih.hidrocarburos.gob.mx/ (accessed Mar 23, 2022).
(25) Gatebe, C. K.; Wilcox, E.; Poudyal, R.; Wang, J. Effects of Ship Wakes on Ocean Brightness and Radiative Forcing over Ocean. *Geophys. Res. Lett.* **2011**, *38* (17), na.
(26) Molod, A.; Takacs, L.; Suarez, M.; Bacmeister, J.; Song, I.-S.; Eichmann, A. *The GEOS-5 Atmospheric General Circulation Model: Mean Climate and Development from MERRA to Fortuna*; NASA TM-2012-104606; NASA, 2012.
(27) Fire Information for Resource Management System. *NASA*. https://firms.modaps.eosdis.nasa.gov/ (accessed Jul 12, 2021).
(28) Shen, L.; Zavala-Araiza, D.; Gautam, R.; Omara, M.; Scarpelli, T.; Sheng, J.; Sulprizio, M. P.; Zhuang, J.; Zhang, Y.; Qu, Z.; Lu, X.; Hamburg, S. P.; Jacob, D. J. Unravelling a Large Methane Emission Discrepancy in Mexico Using Satellite Observations. *Remote Sens. Environ.* **2021**, *260*, 112461.
(29) Brown, P. F.; Saunier, S.; Simon, M.; Heras Cruz, B. *Overview of Methane Detection and Measurement Technologies for Offshore Applications*; Carbon Limits A.S., 2020.
(30) Gatebe, C. K.; King, M. D. Airborne Spectral BRDF of Various Surface Types (Ocean, Vegetation, Snow, Desert, Wetlands, Cloud Decks, Smoke Layers) for Remote Sensing Applications. *Remote Sens. Environ.* **2016**, *179*, 131−148.
(31) Landgraf, J.; Lorente, A.; Langerock, B.; Kumar Sha, M. *S5P Mission Performance Centre Methane [L2__CH4____] Readme*; Document Number Issue 2.1; Tropomi, ESA, 2021.